Experimental Evidence of the Effectiveness and Applicability of Colloidal Nanosilica Grouting for Liquefaction Mitigation

Erminio Salvatore, Ph.D.[1]; Giuseppe Modoni, Ph.D.[2]; Maria Cristina Mascolo, Ph.D.[3]; Davide Grassi[4]; and Giovanni Spagnoli, Ph.D.[5]

Abstract: The low viscosity and the ability to control solidification rate make colloidal nanosilica grout an excellent ground-improvement solution which is functional for different engineering purposes. A comprehensive experimental programme was performed to test the effectiveness and applicability of low-pressure injection of aqueous nanosilica suspensions against seismic liquefaction and to provide the experimental basis for the design, execution, and control of treatments. Scanning electron microscope and X-ray diffraction tests carried out on samples prepared with variable dosages enabled analysis of the microstructure of the original material and grouted sand. The influence of the grout composition on the solidification rate, viscosity, and shear strength of the treated sand was evaluated with preliminary tests to optimize the use of material. The efficacy of treatment in terms of stress–strain response and liquefaction resistance was investigated with a series of drained monotonic and undrained cyclic triaxial tests. A quality control procedure based on sonic wave transmission was established by performing bender element tests on samples cured for different times. The intent was to find the trade-off between a cost-effective use of materials and the mechanical performance of the treated sand. **DOI: 10.1061/(ASCE)GT.1943-5606.0002346.**

Author keywords: Liquefaction mitigation; Colloidal nanosilicate; Low-pressure grouting; Control.

Introduction

Recent experiences such as the earthquakes in Christchurch, New Zealand in 2010/11; Tohoku Oki, Japan in 2011; Emilia Romagna, Italy in 2012; and Palu, Sulawesi, Indonesia in 2018 demonstrated the impact that earthquake-induced liquefaction may produce on the life and economy of the communities living in susceptible areas (Cubrinovski 2013; Chiaradonna et al. 2018b). The phenomenon can heavily damage infrastructures (e.g., roads and pipelines, D'Apuzzo 2019) and buildings even at relatively moderate earthquake intensities (Bird and Bommer 2004; Fioravante et al. 2013). As a remarkable example, the liquefaction caused in Christchurch by the February 22, 2011 earthquake affected nearly 60,000 residential buildings and horizontal infrastructures over one-third of the city area, about 15,000 families lost their homes and 8,000 were permanently displaced, and 900,000 t of liquefied soil were removed from the ground surface after the events (Canterbury Development Corporation 2014; Tonkin + Taylor 2016). During the 2011 Great East Japan earthquake, approximately 27,000 houses, more than 2,000 levees, and several ports suffered damage from the resulting ground liquefaction (Bhattacharya et al. 2011; Yasuda et al. 2012).

The liquefaction phenomenon is well known, and is caused by seismic waves that travel through loose sands and activate volume contraction that, in saturated conditions, results in the accumulation of excess pore water pressures. With limited drainage, pore pressure may equalize the total overburden stress and reduce the effective stresses o a point at which the sand matrix loses its shear resistance and starts behaving like a viscous fluid (Wang et al. 2019). Even without reaching such an extreme condition, the reduction of effective stresses below buildings may cause noticeable displacements and, eventually, a reduction of the bearing capacity of the foundation (e.g., Bray and Macedo 2017; Modoni et al. 2019).

Because liquefaction is governed by different concurrent factors, i.e., nonplastic soil in a loose state, saturation, and partial or no drainage, various mitigation actions may be undertaken to prevent it (JGS 1998; Han 2015; Chiaradonna et al. 2018a). The mobility of grains and their tendency to contract upon cyclic loading may be reduced by dynamically compacting (Mayne et al. 1984), vibrating (Kirsch and Bell 2012; Kirsch and Kirsch 2016), or blasting (Lyman 1941) the soil. Alternative solutions consist of bonding the sand grains with precipitated calcite (Burbank et al. 2013; Xiao et al. 2018a; Consoli et al. 2018), the addition of finer plastic materials (El Mohtar et al. 2013; Huang and Wang 2016), the prevention of excess pore pressure build-up with induced partial

[1]Postdoctoral Researcher, Dept. of Civil and Mechanical Engineering, Univ. of Cassino and Southern Lazio, via G. Di Biasio 43, Cassino 03043, Italy (corresponding author). ORCID: https://orcid.org/0000-0003-0578-381X. Email: e.salvatore@unicas.it

[2]Associate Professor, Dept. of Civil and Mechanical Engineering, Univ. of Cassino and Southern Lazio, via G. Di Biasio 43, Cassino 03043, Italy. ORCID: https://orcid.org/0000-0001-9200-2502. Email: modoni@unicas.it

[3]Assistant Professor, Dept. of Civil and Mechanical Engineering, Univ. of Cassino and Southern Lazio, via G. Di Biasio 43, Cassino 03043, Italy. Email: mc.mascolo@unicas.it

[4]Project Manager Underground Construction, BASF Construction Chemicals Italia Spa, Viale Vicinale delle Corti 21, Treviso 31100, Italy. Email: Italydavide.grassi@basf.com

[5]Global Project and Technology Manager Underground Construction, BASF Construction Solutions GmbH, Dr- Albert-Frank-Str. 32, Trostberg 83308, Germany. ORCID: https://orcid.org/0000-0002-1866-4345. Email: giovanni.spagnoli@basf.com

Note. This manuscript was submitted on July 8, 2019; approved on May 13, 2020; published online on August 3, 2020. Discussion period open until January 3, 2021; separate discussions must be submitted for individual papers. This paper is part of the ***Journal of Geotechnical and Geoenvironmental Engineering***, © ASCE, ISSN 1090-0241.

desaturation (Yegian et al. 2007; Mele et al. 2018), or horizontal and vertical drains (Chang et al. 2004). Another possible strategy to prevent the onset of liquefaction and its impact on superstructures consists of reinforcing foundations with piles, columnar or lattice wall inclusions created with jet grouting (Yamauchi et al. 2017), deep soil mixing (Nguyen et al. 2012), or stone columns (D'Appolonia 1954). Reinforcement aims to reduce shear strains in susceptible soils and transfer loads to deeper, nonliquefiable strata.

As with any ground-improvement application, the most suitable technique should be chosen by scrutinizing the problem from different perspectives. Mechanical effectiveness is certainly the priority, but executability, durability, and cost-effectiveness are important as well. Additionally, the invasiveness of the solution should be considered seriously in the case of pre-existing structures. Whatever the chosen technique, international standards, e.g., ENV 1997-1 (CEN 2004), state as a basic principle that "the effectiveness of the ground improvement shall be checked against the acceptance criteria by determining the induced changes in the appropriate ground properties." Although it is general, this sentence outlines a strategy that may adopted to develop a consistent framework with the three phases of ground-improvement application, i.e., design, execution, and control (Croce et al. 2014). Therefore, depending on the scope of treatment, the performance should be identified with a property (or more than one) that is originally inadequate and subsequently modified with a ground improvement intervention appropriately designed by means of quantitative analyses. The second relevant issue concerns execution, i.e., the selection of treatment parameters necessary to achieve the prescribed goal. Finally, but not less important, the effectiveness of ground improvement should be proven with simple, fast, reliable, and noninvasive control tests.

Filling of sand pores with clay, bentonite, microfine cement, or other chemical products (Karol 1968; Donovan et al. 1984; Spagnoli 2018) has been proven to reduce the liquefaction tendency of sandy soils. However, seepage of these materials through the intergranular voids, mostly in the case of finer soils, may be problematic to the point that the effectiveness of the techniques is inhibited. Nanotechnology provides geotechnical engineers with nontoxic low-viscosity fluids that can be adopted conveniently as alternatives to the aforementioned materials. Nanosilicate grout, normally commercialized as a water suspension of submicrometric silica particles, possesses a low viscosity that allows it to permeate with relative ease into liquefiable soils (Gallagher and Mitchell 2002). Immediately before injection, the suspension is mixed with an activator that reduces the repulsive action among solid particles and triggers the formation of a stable gel made of highly hydrophilic chains of silica particles (Yonekura 1996). Adjusting the relative proportions of nanosilica suspension and activator (Agapoulaki and Papadimitriou 2018) enables control of the gelling speed and seepage that, together with the injection pressure, control the extension of the grouted soil portion.

Nanosilica grout has been used as a fast remediation to stop piping in underground excavations (e.g., Manassero and Di Salvo 2012; Traldi and Levanto 2016) or for sealing contaminants (e.g., Persoff et al. 1994; Moridis et al. 1996). Beneficial effects in terms of improved liquefaction resistance of sandy soils have been observed by several authors (e.g., Gallagher 2000; Gallagher and Mitchell 2002; Liao et al. 2003; Porcino et al. 2011). In this application, ground improvement is produced by the occlusion of intergranular spaces that reduces the grain mobility and contraction tendency of the soil upon cyclic shear, as shown by drained triaxial tests performed by Porcino et al. (2011), who found an increase of soil dilation and peak resistance of the treated sand. A weak bonding among grains cannot be excluded, because tests carried out on pure silica gel by Liao et al. (2003) and Towhata et al. (2008) found uniaxial compression strengths on the order of a few kilopascals.

Considering the executability of treatments, Iler (1979) and Agapoulaki and Papadimitriou (2018) found that the rheological properties of the material in the state transition from suspension to gel depend on the composition, temperature, and pH. Gallagher and Lin (2009) and Hamderi and Gallagher (2013) conducted small-scale experiments and numerical modeling to determine the propagation of the nanosilicate suspension under given hydraulic boundary conditions and the homogeneity of the treated material.

The reduction of liquefaction potential and the transport of nanosilica grout through the soil pores depend significantly on the composition of the grout, as determined by the initial mix of solid silica, water, and activator, and on the progressive dilution of the injected product with groundwater. Among the aforementioned factors, the fraction of solid nanosilica is one of the most crucial, because it affects the cost and thus dictates the economic convenience of treatments. On the one hand, grouts richer of nanosilica could be more effective from a mechanical viewpoint; on the other hand, the increased expense could render this ground-improvement solution inconvenient. The question becomes even more complex considering that the solidification rate of the injected product and consequently the seepage distance of grout depend on the amount of activator added in the admixture. A trade-off thus should be sought among the different components to balance mechanical efficiency, practical executability, and cost-effectiveness of treatments. With a few exceptions (e.g., Persoff et al. 1999), previous studies focused only on the influence of grout composition on the reduction of liquefaction potential, on the rheological properties of the grout, or on the transport of nanosilicate grout through the soil. The present study examined these aspects simultaneously with a comprehensive laboratory investigation to provide the experimental basis to optimize the design, execution, and control of treatments. Different standard and nonconventional laboratory tests were carried out on samples of pure grout and sand–grout mix prepared with various assortments of components to quantify the influence of the solid nanosilica and activator fractions on the stress–strain response of the treated soil, on the reduction of liquefaction potential, and on the fluid-solid phase transformation of the grout. An experimental procedure based on bender elements tests was implemented to prove the effectiveness of sonic tests as a tool for quality control on site.

Properties of Materials

Nanosilica Grout

The grout adopted was a water suspension of nanosilica particles (BASF Chemicals 2017), maintained in a colloidal state with the addition of sodium ions (Na^+), that had a pH value of about 10 and the conditions for isometric nanoparticles of 2–100 nm to be formed [Fig. 1(a)]. The viscosity of the fluid in this state is about 10 m Pa · s, i.e., 10 times higher than the viscosity of water, and this makes the suspension extremely suitable for injection in low-permeability sands. When mixed with an activator consisting of a 10% sodium chloride water solution (pH $\approx$ 7), the pH reduction and the presence of salt destabilises the colloids and lead to polymerize complex and highly hydrophilic silica chains (Iler 1979; Hench 1998; Pedrotti et al. 2017) grouped in the form of spherical silica particles (SOLS). The gel structure, analyzed by X-ray diffraction (XRD) tests, can be defined as amorphous because the few peaks in Fig. 1(b) correspond to diffraction angles typical of the activator salt (NaCl, i.e., halite) (Klug and Alexander 1974).

Although the drying process necessary to perform scanning electron microscope tests (SEM) produces shrinking and cracking

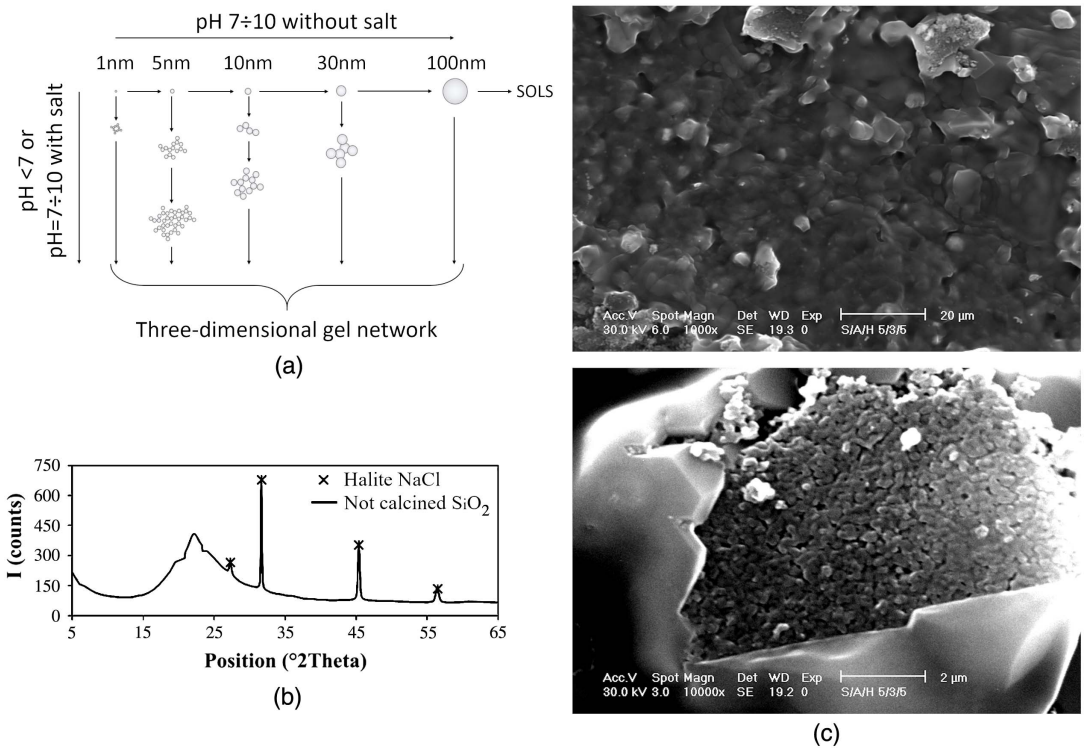

Fig. 1. Microstructural and chemical analyses of the nanosilica gel: (a) scheme of gelling in different conditions (adapted from Iler 1979); (b) X-ray diffractometry; and (c) scanning electron microscopy at different magnifications.

of the xerogel, the SEM images taken at two different magnifications showed that the silica gel formed a matrix of microscopic bubbles with radii on the order of few to 10 μm [Fig. 1(c)] that incorporates the sand particles and occupies the intergranular pores. Because the matrix is made of nanosilica chains and water, it is interesting to evaluate how the fraction of solid silica influences the properties of the material before, during and after solidification. In principle, the amount of solid silica can be regulated diluting the original product with water, but it must not be ignored that dilution influences the reactions between silica and activator. Modification of the relative proportions of these two components influences the gelling speed, varying the time from a few minutes to several hours. This issue was investigated with a test procedure proposed by Persoff et al. (1999). Small cylindrical samples were prepared by mixing water, solid silica, and activator in different proportions and cured at constant environmental conditions ($T = 20$°C). At regular time steps, the containers were rotated to evaluate the physical state of the gel with respect to a scale proposed by Sydansk (1990), in which 1 denotes nondetectable gel, 5 denotes barely flowing gel, and 11 denotes solid gel [Fig. 2(a)]. Fig. 2(b) summarizes the outcomes of this test, and shows the gelling time necessary to reach state 11 on the preceding scale (T_{gel}) for suspensions prepared with different concentrations of solid silica and salt. In these tests, the fraction by weight of solid silica in the solution (w_s) was 3%, 5%, and 10%, and mixed with a fraction of solid salt (w_{NaCl}) between 1% and 20%. The solidification time changed significantly with the grout composition, and was very low (on the order of a few seconds) for the highest solid silica content (10%) and activator (10%), and much higher (on the order of hours) for the more diluted suspensions [Fig. 2(b)].

Furthermore, for any given concentration of nanosilica, the increase of salt content accelerated the reactions, i.e., reduced T_{gel}, but only to a certain point, after which the gelling time increased [Fig. 2(b)]. Iler (1979) explained this response as an effect of the suspension's acidity, and observed that the reaction speed reaches a maximum for pH values approximately equal to 7. The solidification rate is fundamental for the execution of treatments, because a process that is too fast will inhibit seepage and limit the extension of the treated zone, whereas excessively long gelling time could enhance the dispersion of nanosilica in the groundwater, especially if high natural hydraulic gradients are present in the subsoil. In the latter situation, solidification could be delayed or totally inhibited by the excessive dilution of the solid silica, as found in the present experiments in tests conducted at $w_s = 1\%$ that achieved incomplete gelling after some days.

Butron (2005) performed a laboratory study under controlled stress conditions during the first 5 months of the hardening process to investigate the mechanical properties of nanosilica grout. In particular, Butron evaluated the shear strength of the gel formed mixing nanosilicate and salt solution at different curing times with a series of fall cone tests (Fig. 3). The results showed that the shear strength increased significantly with time, reaching values about 20 times greater than initial values 5 months after the sample preparation.

Sand

The nanosilicate solution was grouted into a uniform sand, with subrounded grains passing a #40 sieve (0.425 mm) and retained on a #80 sieve (0.180 mm) in accordance with ASTM D422 (ASTM 2007) (Salvatore et al. 2017; Iolli et al. 2015). X-ray diffraction analysis showed that grains were composed of quartz (90%–96% fraction by volume) with a minor presence of muscovite [$KAl_3Si_3O_{10}(OH)_2$] and microcline ($KAlSi_3O_8$). Table 1 reports the relevant physical properties of the sand, in which D_{50} is mean diameter, C_u is uniformity coefficient, G_s is specific

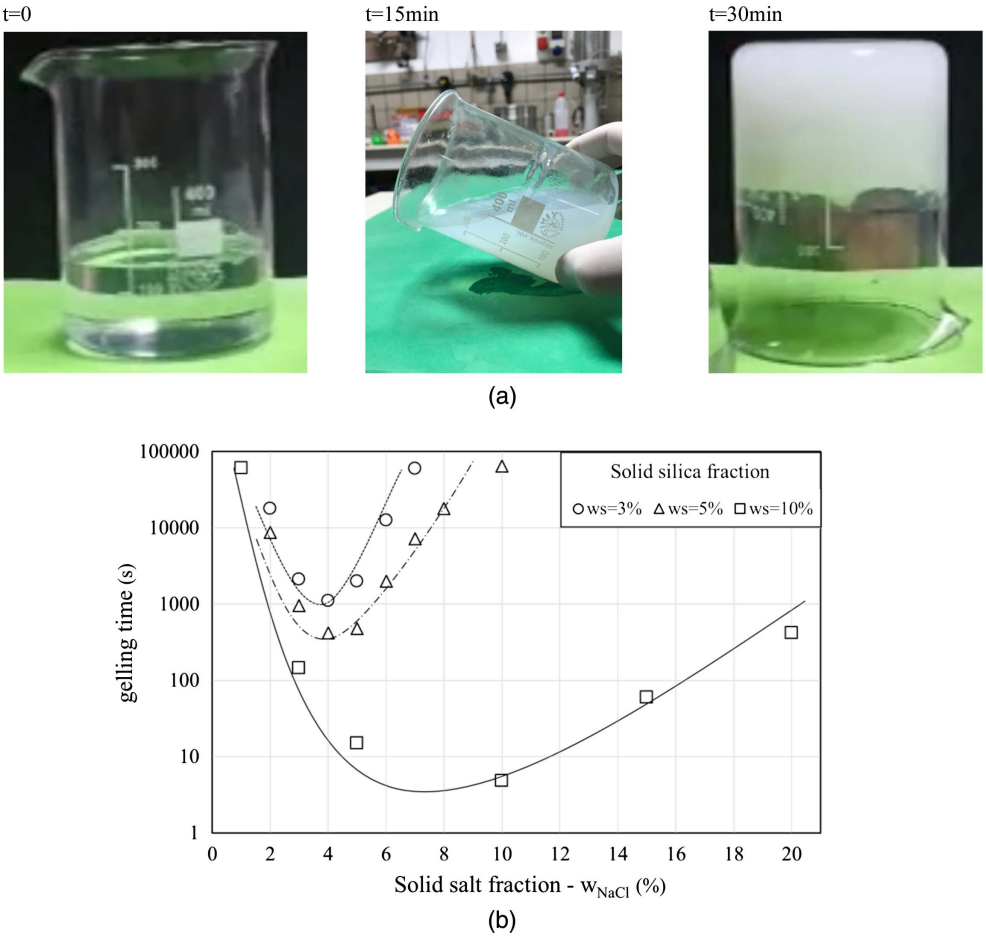

Fig. 2. (a) Example of test performed to estimate the gelling time; and (b) influence of grout composition (w_s = fraction of solid silica in solution; and w_{NaCl} = fraction of solid salt in solution).

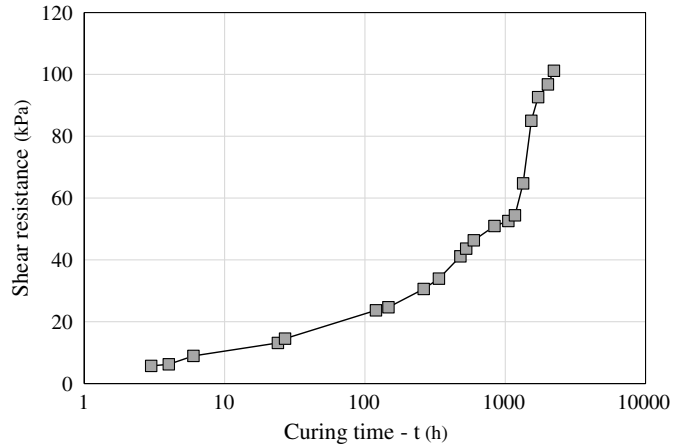

Fig. 3. Fall cone tests of silica gel at different times after sample preparation (adapted from Butron 2005).

Table 1. Physical properties of studied sand

Parameter	Value
D_{50} (mm)	0.303
C_u	1.6
G_s	2.65
e_{min}	0.476
e_{max}	0.821

gravity, and e_{min} and e_{max} are minimum and maximum void ratios, respectively.

Sand–Grout Mix

The treated samples were prepared by pouring dry sand in a mold to form a soil matrix with void ratios higher than 0.75 (corresponding to a relative densities $D_r < 20\%$) and filling the sample with colloidal suspension from the bottom to the top. Seepage was performed until the sand was completely submerged in fluid. Then the samples were enveloped in a thin plastic film and stored for different periods at controlled room temperature (20°C). The composition of the grout was controlled by mixing water, silica suspension, and activator in different proportions. Fig. 4 shows stereophotogrammetric and scanning electron microscope images of the microstructure of the natural and composite materials. Fig. 4(a) shows the clean sand, Fig. 4(b) shows the same sand grouted with a negligible amount of solid silica ($w_s = 1.25\%$), and Fig. 4(c) shows the effects of a larger amount of nanosilica ($w_s = 12.5\%$). The salt content w_{NaCl} in both Figs. 4(b and c) is 2%.

Observation with an optical microscope showed that for the lowest fraction of nanosilica ($w_s = 1.25\%$), the gel in the soil matrix appeared very diluted and transparent, whereas for the larger nanosilica fraction ($w_s = 12.5\%$) the gel appeared milky. The difference was more apparent in the scanning electron microscope images of samples treated with the same silica contents (Table 2) and cured for 24 h at room temperature of 20°C. In these images, the gel appeared exfoliated due to the drying of the samples, which was

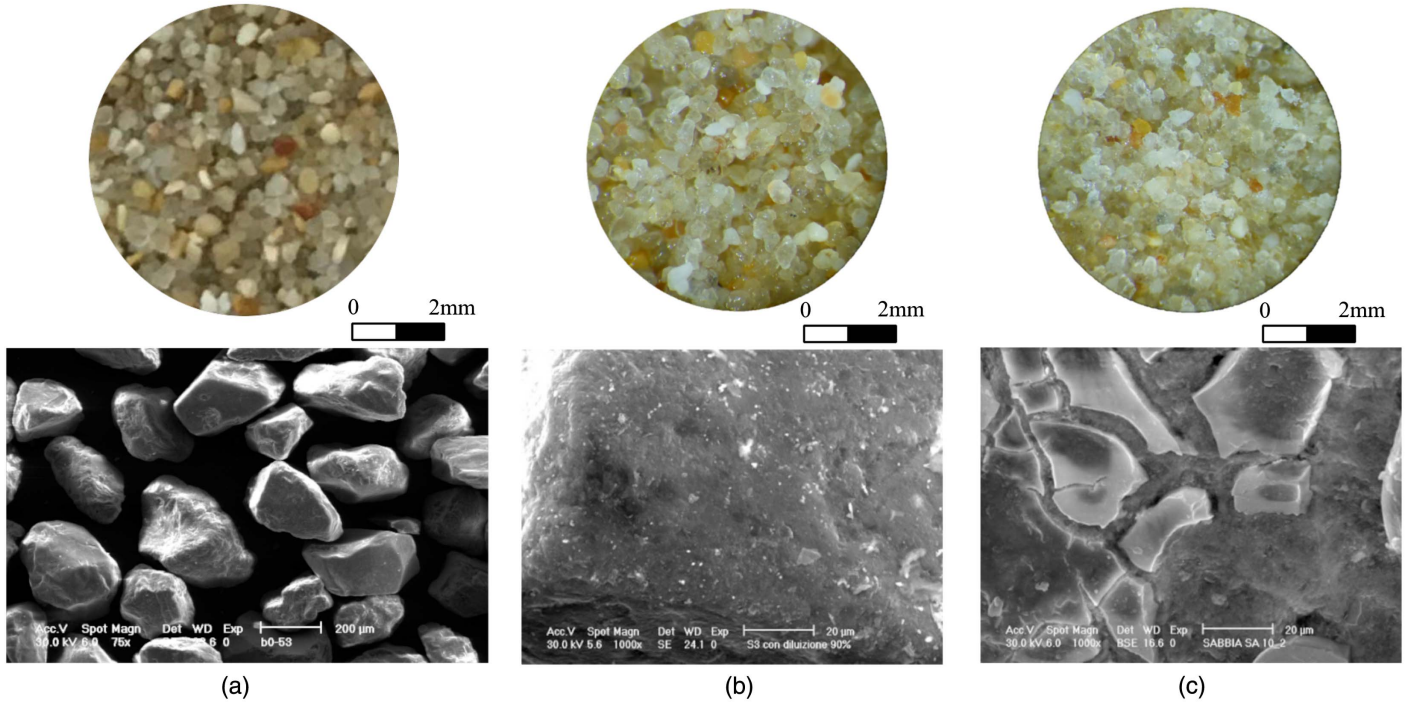

Fig. 4. Stereophotogrammetric and electronic microscope (SEM) images of (a) pure sand; (b) sand treated with grout at 1.25% content of solid silica; and (c) sand treated with grout at 12.50% content of solid silica.

Table 2. Composition of sand samples in Fig. 4 (%)

Sand	Solid nanosilicate fraction, w_s	Activator fraction, w_{NaCl}
Fig. 4(a)	—	—
Fig. 4(b)	1.25	2
Fig. 4(c)	12.50	2

necessary to perform SEM scanning. However, in Fig. 4(b) the sandy grains are uniformly coated with a thin film, whereas Fig. 4(c) shows thicker silicate concretions on the grains' surface. It appears that the function of nanosilica gel is to reduce the mobility of grains by filling the interparticle voids with a semisolid matter and, eventually, to bond the grain contacts (Liao et al. 2003; Towhata et al. 2008). These effects prevent the contraction tendency of soil pores upon cyclic shearing that develops into pore-pressure build-up and eventually liquefaction in undrained conditions. The gel stiffness, which is dependent on the amount of solid nanosilica, could influence the liquefaction resistance of the treated soil.

The preceding observation raises another important question about the minimum amount of nanosilica necessary to reduce the liquefaction potential to the desired level. A preliminary evaluation of the relation between silica content and shear strength of the treated soil, together with its evolution with gelling time, can be derived from a preliminary series of vane tests (ASTM 2000), as was done by Park et al. (2015) and Mori et al. (2018). Several samples were prepared by pluviating dry sand into glass molds [Fig. 5(a)] in a loose state ($e_o \approx 0.8$ and $D_r \approx 0.05$). Samples then were filled with grout prepared with increasing solid silica contents (Table 3), slowly flushing the suspension from bottom to top. At regular curing times, vane shear tests were performed, and the time variation of the resistance was obtained [Fig. 5(b)]. The strength values obtained from these tests must be considered only in relative terms and cannot be used for mechanical analyses, because the experimental conditions (saturation, drainage, and deformation rate) are not controlled (Park et al. 2015; Mori et al. 2018), but this test can be used in routine application for a fast assessment of the soil–gel reactions. In fact, all samples had a significant increase of shear strength compared with the untreated sand [Fig. 5(b), solid circle] and a similar time evolution of this property (the last measurement was performed after 28 days). This result, which also found in previous studies (Yonekura and Miwa 1993; Persoff et al. 1999), indicates that the shear strength increases more than linearly with the solid silica content (w_s). The last column of Table 3 reports the relative increase of strength measured 28 days after the sample formation. This time normally is taken as a reference, but a further slight increase of all curves at longer curing intervals must be admitted. In this study, these tests enabled determining the curing time necessary to perform the triaxial tests on samples representative of the final state, which was fixed at 5 days considering the limited difference between the values corresponding to 5 and 28 days.

Permeation Test

The permeation rate of the grout into the soil and its time evolution due to the change of the rheological properties of the injected fluid are relevant for the execution of treatment. The spacing of injection points and the hydraulic head must be assigned on-site considering the capability of the injected fluid to seep radially and fill the soil volume. This study quantified the evolution of soil-grout permeability with time using equipment that activated seepage through cylindrical samples of sand with diameter and height of 70 and 140 mm, respectively [Fig. 6(a)]. The hydraulic head at the outlet corresponded to the height of the exit hose, whereas the inlet head corresponded to the level in the reservoir. The equipment had two tanks, one containing water and one containing nanosilicate grout. Because nanosilicate grouting for liquefaction mitigation normally

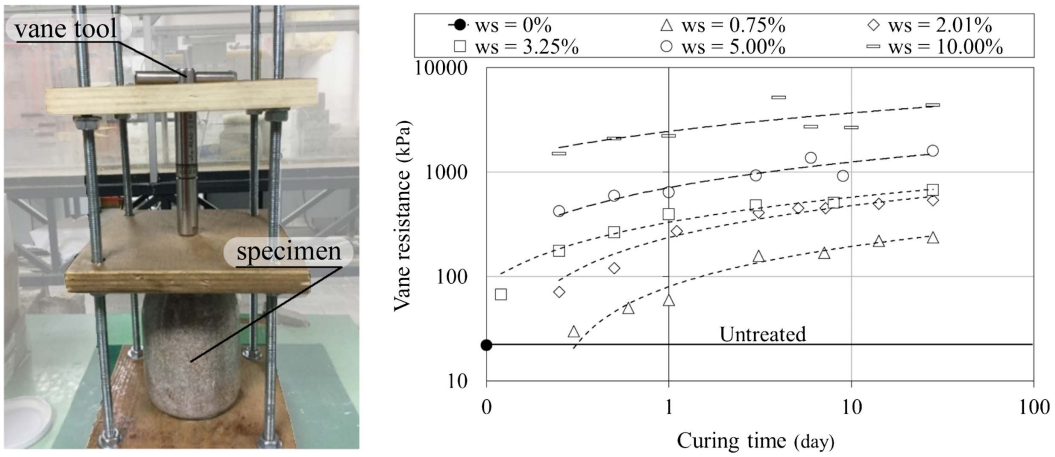

Fig. 5. (a) Laboratory setup of vane test; and (b) evolution with curing time of vane shear strength of specimens treated with grout prepared at different solid silica contents w_s.

Table 3. Composition of grout used for treatment of specimen subjected to vane tests (%)

Fraction nanosilica product in injected grout[a]	Water	Activator	w_s	w_{NaCl}	Increase of vane shear strength at 28 days' curing
5.0	75.0	20.0	0.75	2.0	982
13.4	66.6	20.0	2.01	2.0	2,332
21.7	58.3	20.0	3.25	2.0	2,964
33.3	46.7	20.0	5.00	2.0	7,173
66.7	13.3	20.0	10.00	2.0	19,900

[a]Original product contains 15% solid fraction of nanosilica.

is conducted in saturated soil, permeation tests were carried out in two subsequent phases, first activating the flow of water then activating the flow of nanosilicate grout through the sample. In each phase, the amount of seeping fluid and the feeding hydraulic head were computed by continuously recording the level in the tanks with ultrasonic sensors. The fluid level in the tank and its time evolution then were converted into an equivalent permeability coefficient with the following relation derived from the integration of the transient flow rate in a generic finite time i nterval ($t_0 - t_1$):

$$k = \frac{a \cdot L}{A \cdot (t_1 - t_0)} \ln \frac{h_0}{h_1} \tag{1}$$

where a = cross-sectional area of the supplying tank; A and L = cross-sectional area and length of specimen, respectively; and h_0 and h_1 = initial and final hydraulic heads in measurement time interval (from t_0 to t_1) computed from level of outlet hose.

Whereas the soil–water permeability remains constant with time, the permeability of soil to the nanosilica grout decreases with time due to the increase of fluid viscosity. This phenomenon was quantified for different concentrations of nanosilicate and activator ($w_s = 3\%$–5%, and $w_{NaCl} = 2\%$, 3%, and 5%). The results are reported in Fig. 6(b) plotting versus time the permeability of soil to the grout scaled respect to the permeability of the same sample to the water (k_w ranged between 5×10^{-5} and 2.5×10^{-4} m/s in the different tests)". The outcomes showed that permeability depends significantly on the fluid composition, and decreased more rapidly

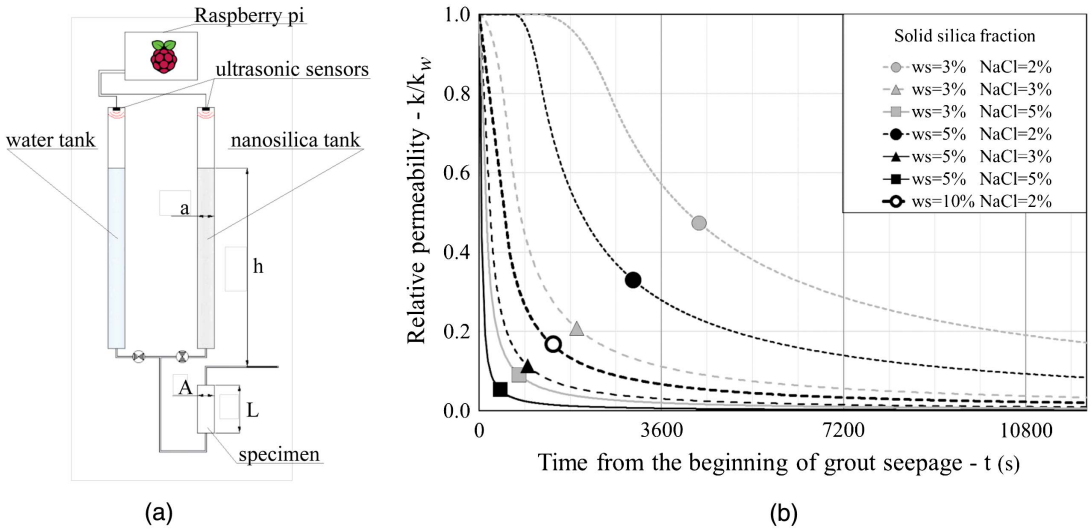

Fig. 6. Seepage tests of nanosilicate grout: (a) testing equipment; and (b) time variation of soil–grout permeability.

J. Geotech. Geoenviron. Eng., 2020, 146(10): 04020108

for larger fractions of solid silica and activator. For the higher salt content ($w_{NaCl} = 5\%$), a very fast decay of permeability occurred independently of the amount of silica, with the result that seepage stopped within a few hundred seconds. The results of Fig. 6(b) can be used to calibrate models simulating grout propagation in saturated porous media (e.g., Bouchelagem and Vulliet 2001) and to predict the dimensions of the soil portion grouted by treatment on-site. In this way, the best composition of grout can be determined in conjunction with the arrays of injection holes, to optimize treatment execution and soil resistance.

Stress–Strain Response

The stress–strain response of the grouted sand was determined from a series of drained monotonic and undrained cyclic triaxial tests of reconstituted cylindrical specimens (diameter of 70 mm and height of 140 mm) with a servocontrolled Bishop and Wesley triaxial apparatus. To investigate the influence of soil density, samples of relatively looser and denser sand were reconstituted with two different procedures: in the first case, dry sand was pluviated in the mold to confer a relative density of approximately 30%, whereas in other cases sand repeatedly was poured into the mold to form layers about 1 cm thick and tamped with a falling weight to reach a relative density of about 60%, following a procedure similar to that suggested by Ladd (1978). After formation, the dry samples were injected with grout. This option was preferred to the presaturation of the soil with water, and was more adherent to site conditions, to control the amount of solid nanosilica in the grout, which influences the mechanical response of treated soil. Particular care was necessary in these tests for the saturation of samples, because this aspect was fundamental for the interpretation of the triaxial tests results. After formation, each sample was flushed from bottom to top with CO_2, then filled from the bottom with nanosilica grout, applying the procedure in Fig. 6(a). The use of CO_2 enabled the adsorption of gas bubbles in the grout, especially because the suspension was prepared by diluting nanosilica and salt in deaired water. To prevent desaturation, the samples were left for 5 days under a level of nanosilica grout at controlled room temperature of 20°C. After this time, the samples were moved carefully to the triaxial apparatus, and the drainage circuits were saturated with water and the pore pressure was increased to 600 kPa. The latter measure was used to dissolve residual air bubbles in the fluid phase and to attain a high degree of saturation (Skempton's B tests performed before each test indicated B-values higher than 0.98).

Drained Monotonic Loading

The mechanical effect of treatment was studied by comparing the results of consolidated drained triaxial compression tests performed on untreated and treated sand prepared at similar void ratios. A first set of results (Fig. 7) produced at increasing confining stresses (100, 200, and 300 kPa) on loose sand ($e_0 = 0.70$–0.75, and $D_r = 0.20$–0.35) treated with $w_s = 5\%$, with the content of salt activator fixed at $w_{NaCl} = 2\%$ in all triaxial tests, showed that the main modification induced by treatment consisted of an increase of dilatancy. This change of behavior, which is consistent with the observations by Porcino et al. (2011), produced relatively

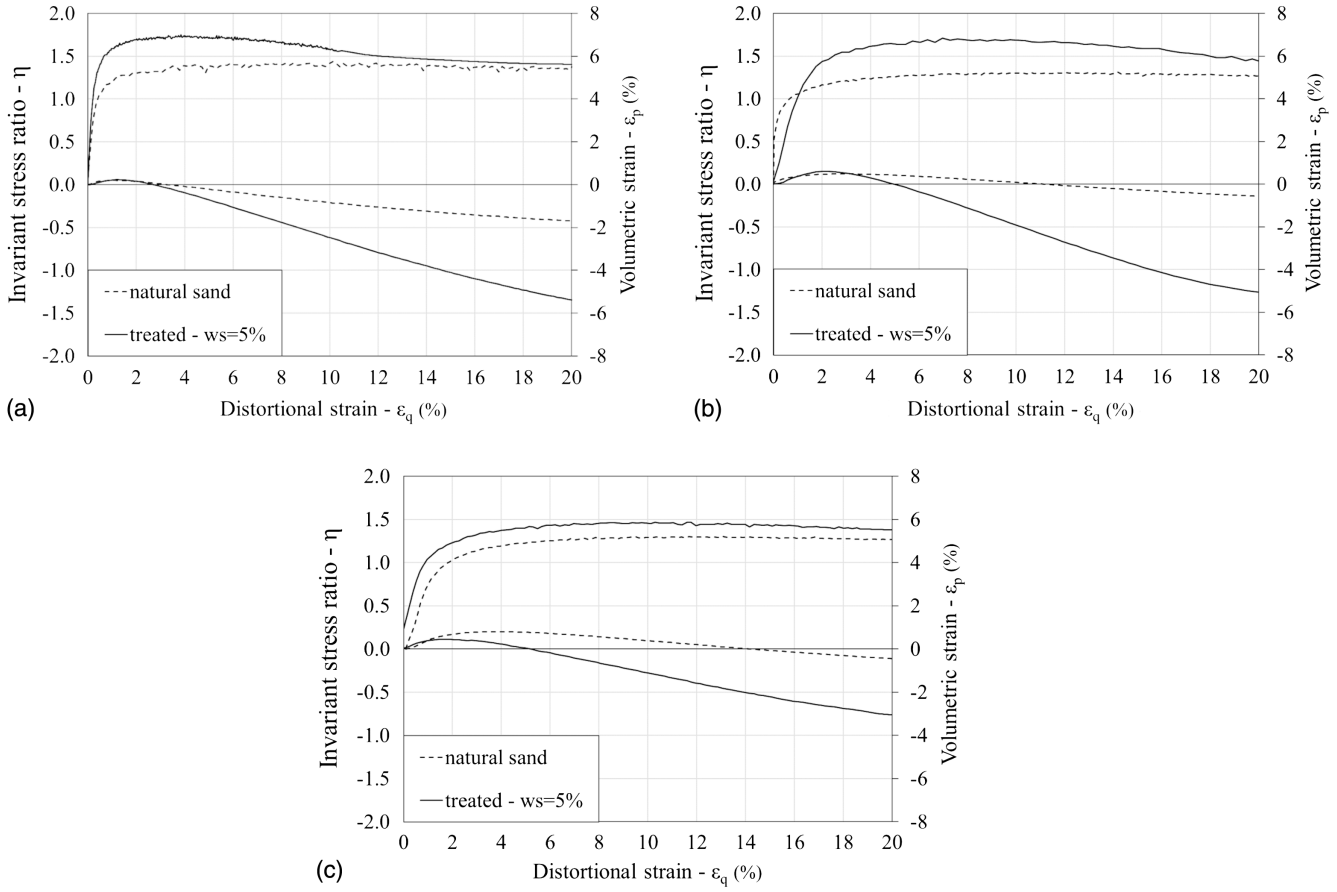

Fig. 7. Consolidated drained triaxial tests performed on loose samples ($D_r = 0.20$–0.35) of natural and treated sand ($w_s = 5\%$ and $w_{NaCl} = 2\%$) at variable confining stresses. Tests were performed after 5 days of curing time: (a) $\sigma'_c = 100$ kPa; (b) $\sigma'_c = 200$ kPa; and (c) $\sigma'_c = 300$ kPa.

J. Geotech. Geoenviron. Eng., 2020, 146(10): 04020108

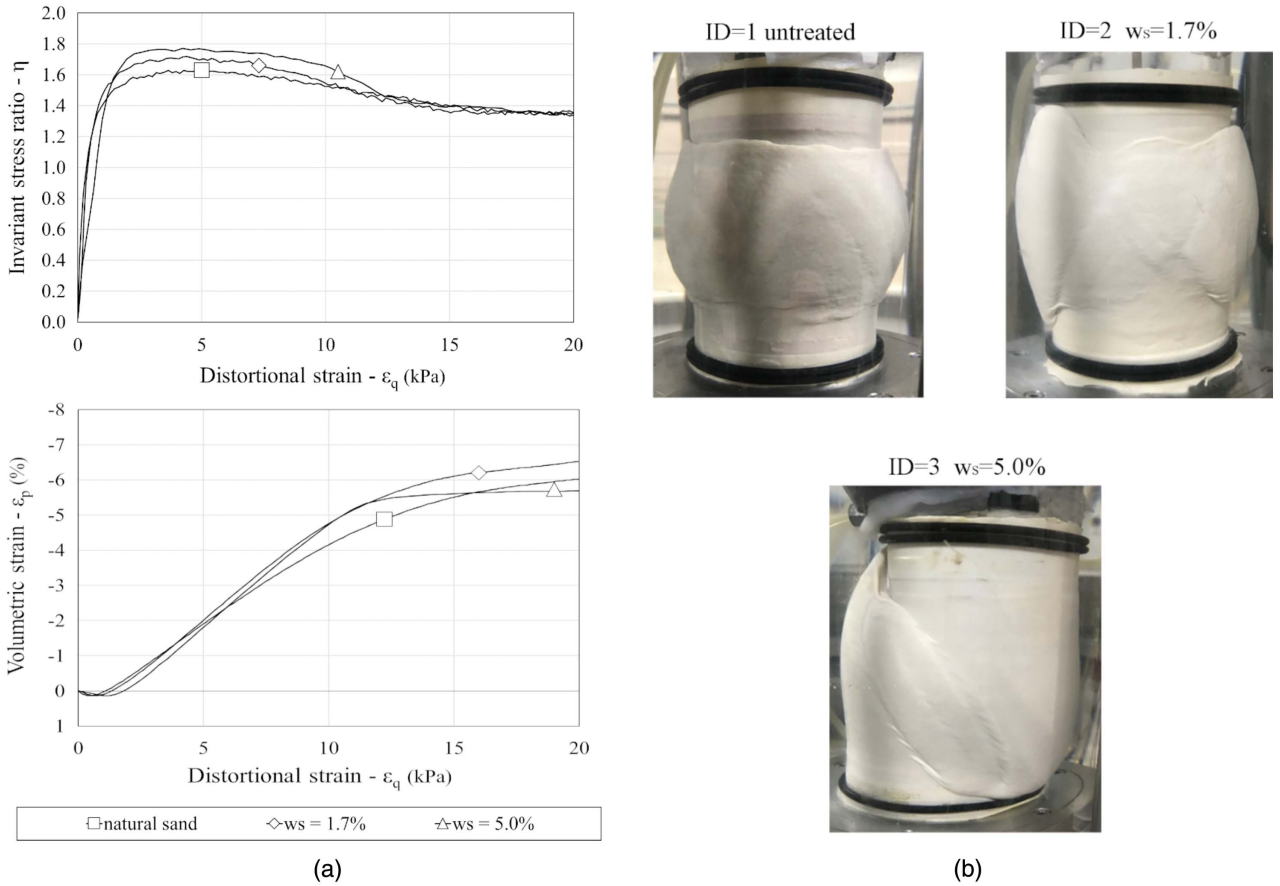

Fig. 8. Consolidated drained triaxial tests performed at 200 kPa confining stress of samples treated with different w_s: (a) stress–stain curves after 5 days of curing; and (b) specimens at end of tests.

small increases of peak stress invariant ratio $\eta = q/p'$) (with differences of 10%–25%). In all tests (untreated and treated sand at any confining stress) there was a tendency to reach a similar ultimate stress ratio, between 1.3 and 1.4. This result suggests that, after its formation in the soil pores, the nanosilicate gel modifies the coupled volumetric–distortional ($\varepsilon_p - \varepsilon_q$) response of the soil, enhancing dilation, but does not affect significantly the ultimate frictional resistance.

The influence of solid nanosilicate content (w_s) on the stress–strain response of the treated soil was determined from the results of three consolidated drained triaxial tests performed at 200 kPa confining stress on samples prepared at an initial relative density of 60% (Fig. 8). The stress strain response of the untreated sample was compared with that of two samples grouted with suspensions containing $w_s = 1.7\%$ and 5.0%. Fig. 8(a) shows an increase of peak stress ratio dependent on w_s with a gradual transition from the untreated to the treated sand with higher silica content. The sand grouted with $w_s = 1.7\%$ was slightly more resistant than the original sand but had a similar continuously dilatant behavior, whereas the sample at the highest nanosilica content ($w_s = 5\%$) behaved in a more brittle manner. This effect, shown by the abrupt decay of deviatoric stress after the peak, was confirmed by the sudden change of rate in the distortional–volumetric strain curve ($\varepsilon_p - \varepsilon_q$), which became suddenly pseudohorizontal, and by the pictures of the samples taken at the end of tests [Fig. 8(b)]. Whereas the untreated sample had the typical barrel shape, the treated specimens tended to localize deformation within narrow portions. The shear bands that appeared at the end of the tests, which were more prominent and concentrated for the highest silica content, are symptomatic of an unstable response typical of very dense (Salvatore et al. 2016, 2018, 2019; Modoni et al. 2018) or cemented (Xiao et al. 2018b) granular material. As in Fig. 7, the similar ultimate stress ratio (equal to 1.35) of all samples indicates that the nanosilica gel had limited effects on the frictional resistance of the material for the considered curing time.

On the other hand, Fig. 9 shows the stress–strain response of samples prepared with the same nanosilicate suspension ($w_s = 5.0\%$) but tested at curing times of 5 and 15 days. Peak strength increased further is the test performed after 15 days of curing, but this effect was not accompanied by a significant increase of dilatancy. Furthermore, unlike the examples in Fig. 8, the increase of strength persisted at the ultimate state ($\eta_{res} = 1.60$ versus 1.35). It is not easy to find a micromechanical cause for this phenomenon that takes place on the shear planes at such large strains. However, it seems logical to relate it to the increase of nanosilicate gel strength with time, shown quantitatively in Fig. 3 (Butron 2005) and empirically perceived as an increase of hardness when touching the gel samples. A possible interpretation could stem from the interlocking of clusters formed by sand grains bonded by nanosilicate matrix, which might induce a larger sliding resistance on the shear planes.

Summarizing the results of Figs. 6–8, different short- and long-term effects of nanosilica grouting occurred in the treated samples. In the short term, the nanosilicate gel clogged the interparticle voids, decreasing the contractive tendency upon shearing, enhancing dilatancy and consequently improving the peak shear resistance of the treated soil. This effect was more pronounced for grouts with higher nanosilica content, possibly due to a higher stiffness of the gel. With time, the solidification process increased the strength of

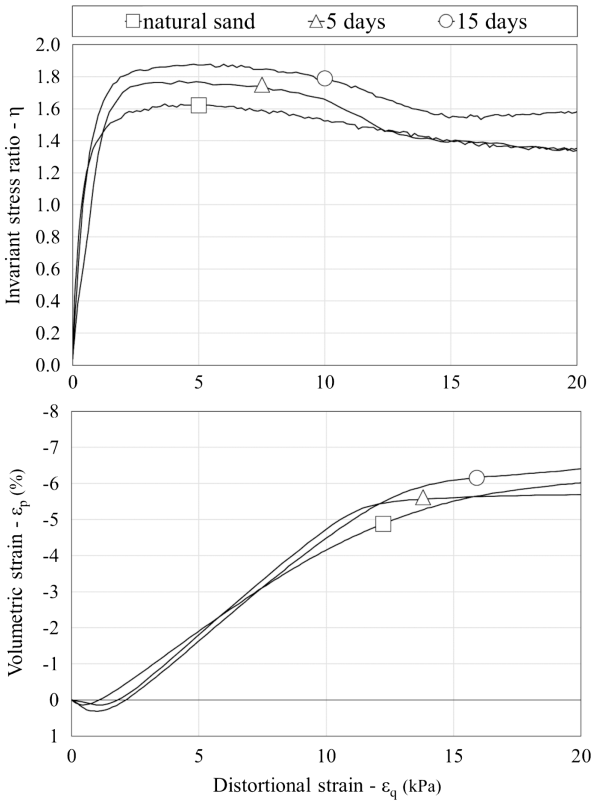

Fig. 9. Tests performed at 200 kPa confining stress of specimens grouted with $w_s = 5.0\%$ nanosilica at different curing times.

the gel (Fig. 3) contributing in this way to enhanced shear resistance of the treated soil.

Undrained Cyclic Loading

The effects of treatment on the liquefaction response of sand are investigated performing undrained cyclic triaxial tests on relatively looser ($D_r \approx 30\%$) and denser ($D_r \approx 60\%$) samples. In both cases, the experiments included tests of untreated and treated soil, in the latter case 5 days after sample preparation. The relatively dense samples were grouted with a suspension with $w_s = 5.0\%$, whereas the looser samples were grouted with $w_s = 5\%$ and 10% to reach in both cases a meaningful reduction of the liquefaction potential. The amount of activator salt, w_{NaCl}, was fixed in all cases at 2%. After 5 days of curing in a controlled environment, the treated samples were transferred to the triaxial apparatus, isotropically consolidated up the mean effective stresses σ'_o in Table 4, and subjected to undrained shearing. The grouting–loading sequence may not be representative of the conditions on site, where soil is subjected to overburden stress, then grouted and eventually shaken by earthquakes. In these tests, the inversion of the consolidation–grouting sequence was necessary because grouting of the soil in the triaxial cell would have clogged the drainage system (consisting of porous stones, pipes, and pore-pressure transducers). Although this modification could in principle make the results not fully representative of the anticipated field performance by altering the fabric and precompressing the grout, after 5 days of curing time the gel only partly had developed its strength and stiffness (Fig. 3), and the limited compressibility of sand would limit the onset of pressure in the grout.

During the shearing phase, deviatoric stress cycles of variable amplitudes Δq were imposed to the specimen (e.g., Fig. 10) at

Table 4. Program of undrained cyclic triaxial tests

ID	e_0	D_{r0} (%)	w_s (%)	σ'_o (kPa)	Δq (kPa)	CSR	n_{liq}	$\varepsilon_{q,\mathrm{peak}}$
1	0.62	58.3	—	100	20	0.10	—	—
2	0.65	49.6	—	100	30	0.15	—	—
3	0.64	52.5	—	100	40	0.20	18	−1.13
4	0.62	58.3	—	100	50	0.25	15	−1.32
5	0.62	58.3	—	100	70	0.35	2	−7.41
6	0.61	61.2	5	100	50	0.25	58	−0.43
7	0.62	58.3	5	100	60	0.30	12	−0.57
8	0.63	55.4	5	100	70	0.35	6	−0.67
9	0.73	26.4	—	100	50	0.25	1	−7.08
10	0.74	23.5	—	200	80	0.20	1	−4.92
11	0.75	20.6	—	200	60	0.15	11	−3.44
12	0.72	29.3	—	200	20	0.05	66	−0.52
13	0.72	29.3	—	200	50	0.13	17	−1.05
14	0.73	26.4	5	200	100	0.25	6	−0.97
15	0.71	32.2	5	200	60	0.15	17	−0.87
16	0.74	23.5	5	200	50	0.13	25	−0.83
17	0.70	35.1	5	200	40	0.10	110	−0.59
18	0.72	29.3	10	200	40	0.10	—	—
19	0.72	29.3	10	200	60	0.15	—	—
20	0.72	29.3	10	200	80	0.20	—	—
21	0.68	40.9	10	200	100	0.25	116	−0.46
22	0.69	38.0	10	200	120	0.30	60	−0.54
23	0.75	20.6	10	200	180	0.45	15	−0.69

constant axial strain rate ($\dot{\epsilon}_a = 5\%/h$), simultaneously measuring the pore pressure increase Δu and computing the pore pressure ratio r_u, defined as the ratio of Δu to the initial mean effective stress σ'_o [Eq. (2)]. Liquefaction triggering was assumed when r_u reached a value of 0.9, as suggested by Ishihara (1993), because this condition critical for the bearing capacity of foundations. Finally, the relation between applied cyclic stress ratio (CSR) [Eq. (3)] and number of cycles (n_{liq}) was used to determining instantaneous values of $r_u = 0.9$ (Table 4 and Fig. 11)

$$r_u = \frac{\Delta u}{\sigma'_0} \tag{2}$$

$$\mathrm{CSR} = \frac{\Delta q}{2\sigma'_0} \tag{3}$$

The efficacy of treatment is preliminarily indicated by the curves of Fig. 10, which are indicative of the results obtained from untreated [Fig. 10(a)] and treated [Fig. 10(b)] sand samples prepared at the same initial relative density ($D_{r0} \approx 0.58$). In both tests, CSR of 0.25 was applied and the evolution of the pore pressure ratio r_u [Eq. (2)] was monitored. Fig. 10 reports the peak r_u values corresponding to each cycle. The different behavior of the two materials evidently was due to the different history of pore-pressure build-up, which was much slower in the treated soil due to the presence of nanosilica gel in the interparticle pores, which limited grain mobility and volume contraction. Therefore, it is sufficient to look at the initial part of the curve in the effective stress invariant plane (p'-q), which shows a contractive (leftward) and dilative (rightward) tendency in the natural and the treated sand, respectively. As a consequence, the natural sand reached $r_{u\_\mathrm{peak}} = 0.9$ at the 15th cycle and then underwent complete liquefaction (zero mean effective stress p') at the 19th cycle, whereas the treated material reached $r_{u\_\mathrm{peak}} = 0.9$ at the 58th cycle but always preserved positive mean effective stress p' in the subsequent loading–unloading (cyclic mobility). During these cycles, the stress–strain curves always had a positive tangent stiffness and the stress–strain loops were significantly stiffer and narrower. These results are particularly

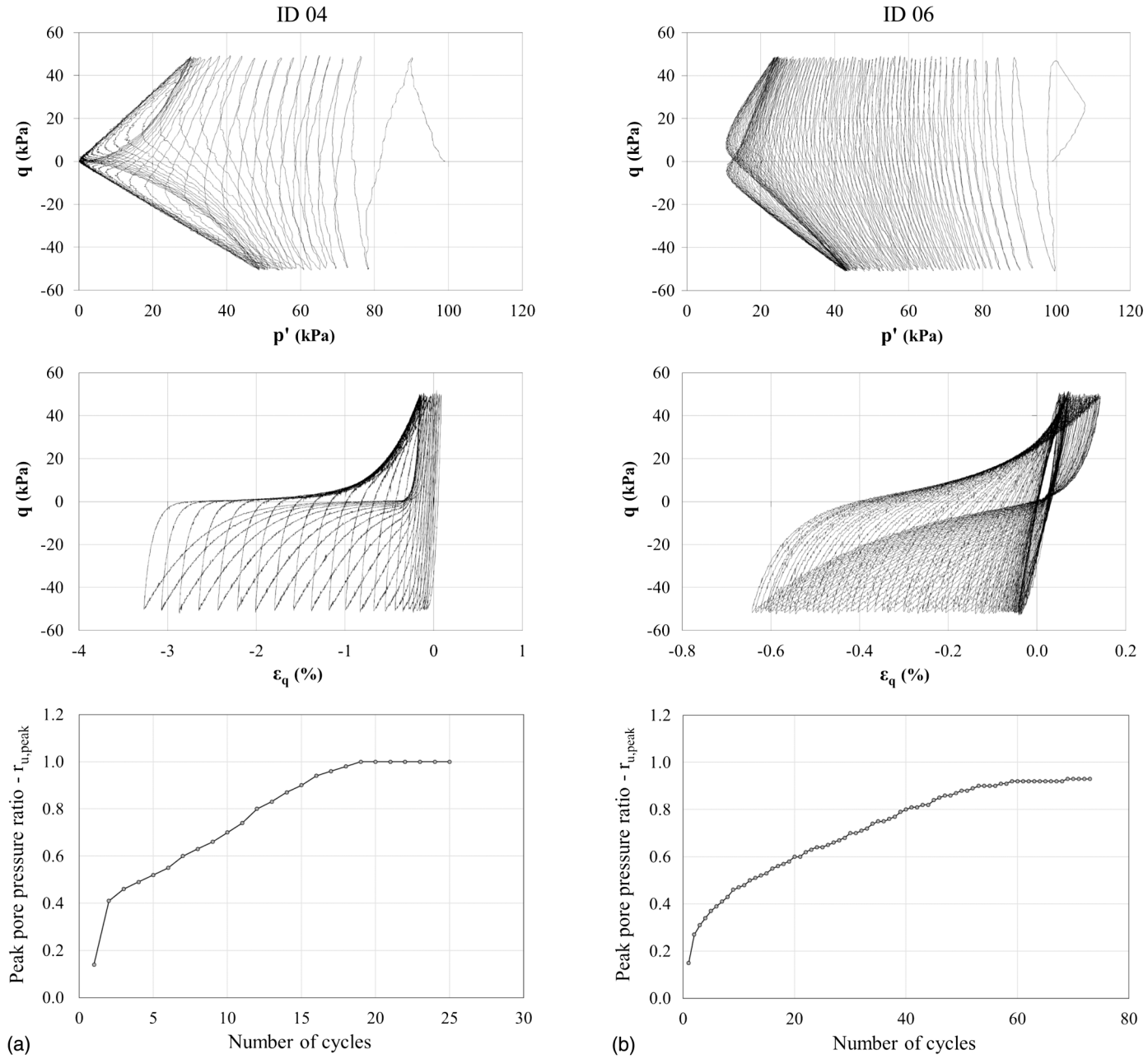

Fig. 10. Results of cyclic undrained triaxial test performed with CSR = 0.25 of relatively dense soil ($D_r = 58\%$): (a) natural soil (Table 4, ID4); and (b) grouted soil (Table 4, ID6).

relevant for the performance of the improved ground, because deformability is a critical issue for the performance of foundations.

The preceding effects occurred repeatedly in all tests, as summarized in Table 4 for samples prepared at different initial densities with variable nanosilica contents. In general, there were a comparatively larger number of cycles and lower absolute distortional strains for the treated soil at the assumed triggering condition ($r_{u\_peak} = 0.9$). The number of cycles producing liquefaction (n_{liq}) is plotted versus the applied cyclic stress ratio CSR in Fig. 11 with hollow symbols, whereas solid symbols represent the highest CSR for which liquefaction did not occur. This representation is particularly relevant for the design of treatment because it enables calibrating advanced constitutive models (e.g., Bullock et al. 2018) or computing the safety factor with simplified methods in which CSR and n_{liq} respectively are related to the intensity and magnitude of earthquake causing liquefaction (e.g., Boulanger and Idriss 2014). The experimental points obtained for each combination of relative density and nanosilica content were fitted with power function curves, and the inferred relations are given in the plot (Seed et al. 1975; Green and Terri 2005). In general, coefficients and exponents of this function are comparable to those found by previous authors for natural soils (e.g., Xiao et al. 2018a, 2019), and the exponents were larger for the denser material, consistent with the observations of Boulanger and Idriss (2014). In both cases, the effect of treatment consisted of an upward shifting of the curves, without a meaningful change in terms of slope, but a distinction is necessary between looser and denser soil [Figs. 11(a and b)]. The denser sand initially had fairly good liquefaction resistance (the cyclic stress ratio corresponding to 15 cycles was $CSR_{15} = 0.22$), which increased significantly with nanosilica grout at $w_s = 5\%$

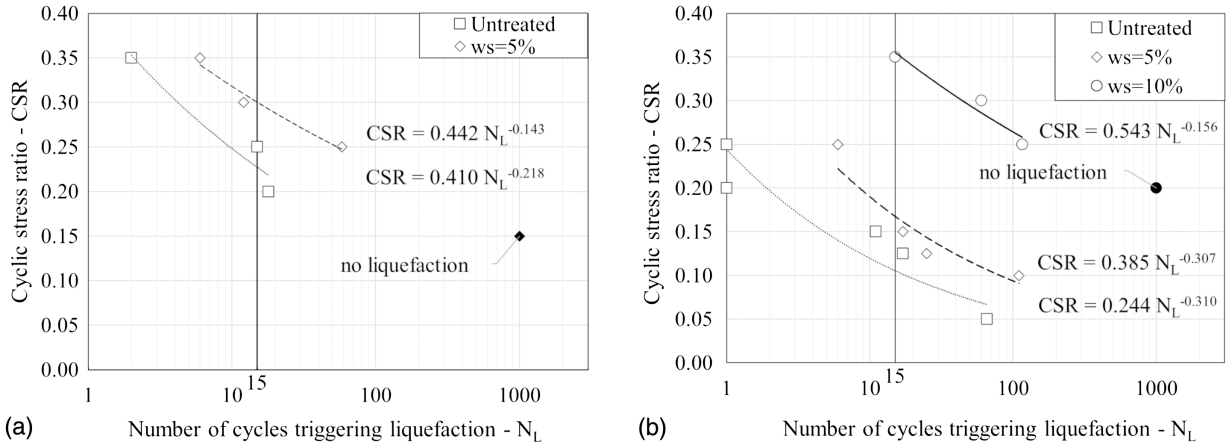

Fig. 11. Improvement of liquefaction resistance of sand with variable w_s: (a) relatively dense sand (D_r = 50%–60%); and (b) relatively loose sand (D_r = 20%–40%).

(CSR_{15} = 0.30); the looser sand had much lower original liquefaction resistance (CSR_{15} = 0.12), but its increase obtained with w_s = 5% nanosilicate was limited (CSR_{15} = 0.15). Therefore, because w_s = 5% grout was not adequate to neutralize the contraction tendency of the looser soil upon cyclic shearing, additional tests were performed by grouting the looser sand with a solid silica fraction w_s = 10%, and more-satisfactory results were obtained (CSR_{15} = 0.45). Apart from showing the dependency of the liquefaction resistance on the composition of grout, the preceding tests outline a design strategy to choose a convenient dosage of components in relation to the seismic demand of the site.

Quality Control

As with any ground-improvement technique (e.g., CEN 2004), the efficacy of nanosilicate grouting must be proven with tests that confirm a correct execution of the process (quality assurance) and the conformity of the product to the standards defined in the project (quality control). For nanosilicate grouting, the former tests may consist of ensuring the quality and composition of the injected grout and the regular execution of injection. The latter tests are aimed at identifying possible defects of the grouted material. For this second aim, a laboratory technique based on the shear wave propagation was implemented, equipping the previously described triaxial apparatus with bender elements (Lee and Santamarina 2005). This technique currently is adopted for testing the efficacy of other ground-improvement methods such as microbial-induced calcite precipitation (e.g., Mortensen and Dejong 2011). The principle tested herein of wave propagation is thought to be extendable in real applications with the adoption of consolidated sonic techniques (down-hole, cross-hole, and so forth). Since its early conception (Shirley and Hampton 1978; Dyvik and Madshus 1985), the bender element technique has gained increasing popularity due to its fast execution. In this experimental campaign, cantilever piezoceramic transducers were positioned in the bases of the samples to generate sonic waves of assigned frequencies and to the record arrival time in order to calculate propagation speed. Despite the simplicity of the principle, the identification of the shear wave arrival at the receiver may be troublesome due to shear wave interactions with compressional waves (Modoni 1997). However, performing tests with various frequencies enables distinguishing compression and shear waves (e.g., Ferreira et al. 2019; Irfan et al. 2019) and identifying more correctly their respective travel times. An example of tests performed in this study (Fig. 12) showed that it is very difficult to identify the arrival time of the shear waves with the lowest frequency (2.5 kHz), because of the superposition with lower-amplitude signals given by faster compressional waves (Arroyo et al. 2003). Increasing the excitation frequency (e.g., to 10 and 50 kHz) enabled amplifying the compressional waves and thus identifying their arrival time with more confidence. The arrival time of the shear wave is identified in Fig. 12 at the first meaningful peak of the cross-correlation function computed between the low-frequency (2.5 kHz) input and output.

Fig. 13 shows an example of compressional and shear wave velocity measurement performed during a test of natural sand. In this test, the sample underwent isotropic compression, and bender elements tests were performed at increasing stress levels. This procedure enabled validating the adopted interpretation criterion and better identifying the modification of the soil response. The two plots show that the compressional wave velocity was independent of the effective stress, and basically was dictated by the higher volumetric stiffness of the water. In contrast, the shear wave velocity had a clear dependency on the effective stress. To investigate the

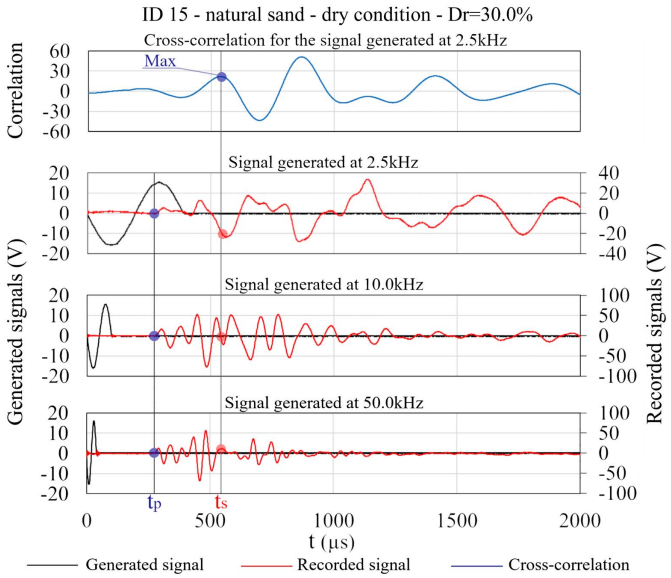

Fig. 12. Example of measurement with bender elements.

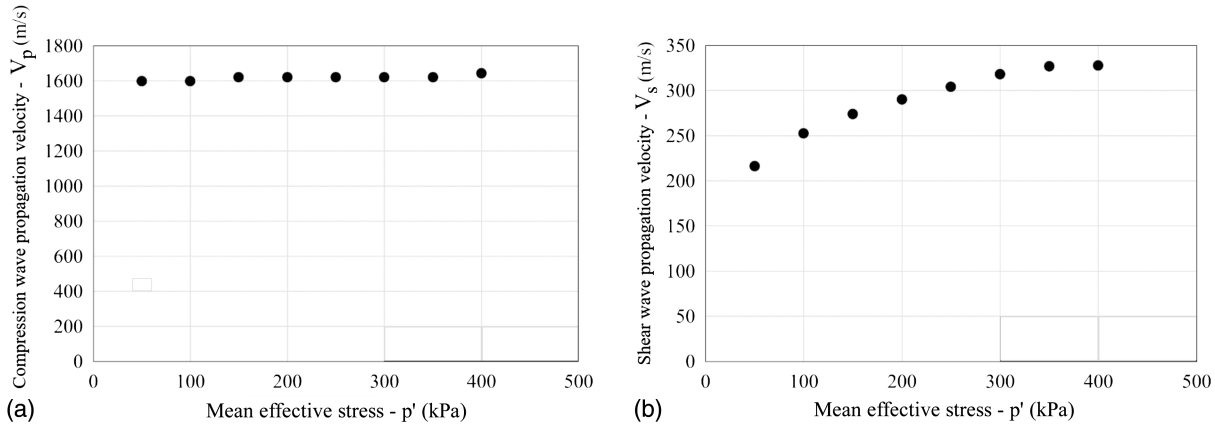

Fig. 13. Measurements of compressional and shear wave velocity during test of untreated soil ($D_r \approx 30\%$).

efficiency of grouting, the tests were repeated on a sample prepared at almost the same relative density ($D_r \approx 30\%$) and treated with nanosilicate grout prepared at $w_s = 5\%$. The treated sample was left in the triaxial cell for 24 days after its formation. During this period, cycles of consolidation (loading and unloading the mean effective stress between 50 and 400 kPa) periodically were carried out. During each cycle, bender element tests were performed to measure the shear wave velocity and values were obtained at each mean effective stress p' (Fig. 14). The comparison of bender element tests at different p' was preferred to the single measurement carried out at different times with a unique stress state to better appreciate the variation of soil stiffness induced by the inclusion of nanosilica. The comparison with the tests of natural sand showed an evident increase of V_s in the treated soil together with a progression with time. The different curves show that V_s increases faster during the first 9 days, after which then the variation continued at a slower rate for the remaining period. This effect, possibly correlated with the hardening of the nanosilica gel (Figs. 3 and 9), indicates that wave propagation velocity may be an indicator of the treatment effectiveness and the potential of sonic tests for controlling the efficacy of treatments on site.

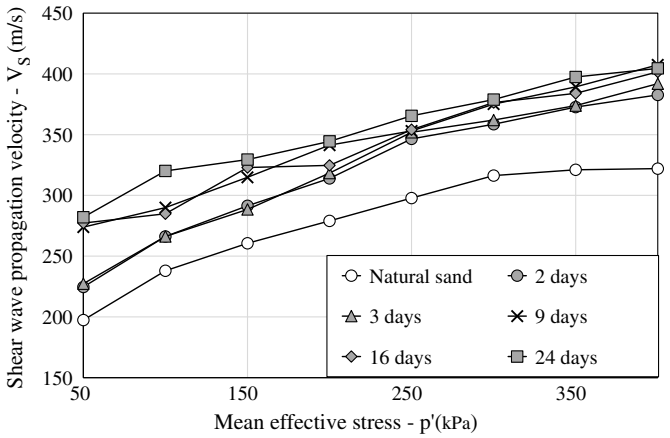

Fig. 14. Shear wave velocity versus mean effective stress of natural sand ($D_r \approx 30\%$) and of a sample at similar relative density treated with nanosilicate grouting ($w_s = 5\%$) at different curing times.

Conclusions

The effectiveness and applicability of nanosilicate grouting to reduce the liquefaction potential of sands was explored to clarify the basic principles governing this ground-improvement application and to outline a strategy for the design, execution, and control of the technique. An experimental program consisting of standard and nonconventional tests was developed. Microscopic observation of the fabric, combined with the phenomenological interpretation of the mechanical tests, enabled determination of the principles ruling the response of the treated material against liquefaction. After the reaction with the activator salt, the nanosilicate forms a gel that occupies the intergranular sand pores. The mobility of grains and the contractive tendency of the sheared sand, which under cyclic conditions are the predisposing factors for liquefaction triggering, are neutralized by the presence of the gel. In the short term, improvement is dictated mainly by a more dilatant behavior of the treated soil, which led to higher peak stress invariant ratios during consolidated drained monotonic triaxial tests. With time, the progressive development of gel strength contributed to the increase of the shear resistance of the treated soil, also at the ultimate state. This significantly depends on the composition of the grout and, primarily, on the solid fraction of silica.

From the viewpoint of design, international standards [e.g., ENV 1997-1 (CEN 2004)] state that "The effectiveness of the ground improvement shall be checked against the acceptance criteria by determining the induced changes in the appropriate ground properties." For liquefaction assessment, there was ample convergence to identify the CSR-n_{liq} function or, equivalently, the cyclic stress ratio corresponding to 15 cycles (CSR_{15}) as the characteristic resistance (e.g., Ziotopoulou and Boulanger 2013). The present study showed that nanosilicate grout is able to increase liquefaction resistance, but also that control of the grout composition is fundamental to achieve the goal in relation to the seismic demand and initial soil properties (i.e., relative density). Because the latter aspect significantly influences the cost, the relation between liquefaction resistance and grout composition is fundamental to the trade-off between technical feasibility and economic convenience of treatments.

To execute treatments, a grid of injection points must be set in the field with an appropriate span to permeate the desired volume with grout. The distance between injection points must be fixed considering the capability of the seepage capability of the grout, which is governed by the time evolution of viscosity. The tests performed enabled quantifying the role of grout composition and, primarily, of the amount of activator salt, w_{NaCl}, on the gelling

time and decay of the soil–grout permeability. The provided data enabled calibrating models simulating the diffusion of grout.

Another important issue is quality control, i.e., the assessment of ground-improvement efficacy. The sonic technique implemented in the laboratory with bender element showed that wave propagation velocity is a good indicator of the treatment effectiveness. Shear wave velocities of grouted soil increased at variable rates with time; the increase was relatively fast in the beginning (0–9 days), but continued for longer periods (up to 24 days in the present analysis) consistently with the development of strength in the nanosilica gel. This result shows the potential of sonic tests for controlling the efficacy of treatments on-site.

The on-site transferability of the preceding results is not straightforward and poses questions that cannot be overlooked, because, moving from laboratory to site, the conditions vary and are not fully controlled. The effectiveness and convenience of treatments relies on the possibility of grout seeping at a meaningful distance from the injection holes and on the polymerization of the nanosilica gel. With regard to seepage, the results of Fig. 6(b) can be extended to other soils types (e.g., more heterogeneous), because the permeability–time functions are scaled with the values of soil–water permeability coefficients. Differences could stem from a faster or slower speed of fluid–solid transformation arising from a different mineralogy of the original soils or from other environmental conditions. The available experimental studies usually refer to silica sand, and thus extension to another sand mineralogy should be ad hoc investigated. However, because nanosilica forms a filler for the sand, application to other sand types (e.g., carbonate) seems feasible. The influence of temperature and pH was investigated by Iler (1979), who found that the reaction speed increases with temperature and varies with the pH, reaching a maximum at pH = 7, and slightly decreasing for values typical of groundwater conditions (i.e., 6–8). These aspects require generalizing the relations found in this work including a dependency on the environmental conditions. More generally, the application on-site of the preceding results requires the experimental validation of propagation models, such as that proposed by Bouchelagem and Vulliet (2001), which represents a next step of the research.

Data Availability Statement

All data, models, and code generated or used during the study appear in the published article.

Acknowledgments

The authors acknowledge the contribution by the EU-funded project LIQUEFACT "Assessment and mitigation of liquefaction potential across Europe: a holistic approach to protect structures/infrastructures for improved resilience to earthquake-induced liquefaction disasters," Project ID 700748, funded under H2020-DRS-2015.

References

Agapoulaki, G. I., and A. G. Papadimitriou. 2018. "Rheological properties of colloidal silica grout for passive stabilization against liquefaction." *J. Mater. Civ. Eng.* 30 (10): 04018251. https://doi.org/10.1061/(ASCE)MT.1943-5533.0002377.

Arroyo, M., D. Muir Wood, and P. D. Greening. 2003. "Source near-field effects and pulse tests in soil samples." *Géotechnique* 53 (3): 337–345. https://doi.org/10.1680/geot.2003.53.3.337.

ASTM. 2000. *Standard test method for laboratory miniature vane shear test for saturated fine-grained clayey soil*. ASTM D4648-00. West Conshohocken, PA: ASTM.

ASTM. 2007. *Standard test method for particle-size analysis of soils (withdrawn 2016)*. ASTM D422-63(2007)e2. West Conshohocken, PA: ASTM.

BASF Chemicals. 2017. "Technical datasheet of MasterRoc MP 325." Accessed November 6, 2017. https://assets.master-builders-solutions.com/it-it/basf-masterroc%20mp%20325%20mar_2020.pdf.

Bhattacharya, S., M. Hyodo, K. Goda, T. Tazoh, and C. A. Taylor. 2011. "Liquefaction of soil in the Tokyo Bay area from the 2011 Tohoku (Japan) earthquake." *Soil Dyn. Earthquake Eng.* 31 (11): 1618–1628. https://doi.org/10.1016/j.soildyn.2011.06.006.

Bird, J. F., and J. J. Bommer. 2004. "Earthquake losses due to ground failure." *Eng. Geol.* 75 (2): 147–179. https://doi.org/10.1016/j.enggeo.2004.05.006.

Bouchelagem, F., and L. Vulliet. 2001. "Mathematical and numerical filtration–advection–dispersion model of miscible grout propagation in saturated porous media." *Int. J. Numer. Anal. Methods Geomech.* 25 (12): 1195–1227.

Boulanger, R. W., and I. M. Idriss. 2014. *CPT and SPT based liquefaction triggering procedures*. Rep. No. UCD/CGM.-14. Davis, CA: Dept. of Civil and Environmental Engineering, Univ. of California at Davis.

Bray, J. D., and J. Macedo. 2017. "6th Ishihara lecture: Simplified procedure for estimating liquefaction induced building settlement." *Soil Dyn. Earthquake Eng.* 102 (Nov): 215–231. https://doi.org/10.1016/j.soildyn.2017.08.026.

Bullock, Z., Z. Karimi, S. Dashti, K. Porter, A. B. Liel, and K. W. Franke. 2018. "A physics-informed semi-empirical probabilistic model for the settlement of shallow-founded structures on liquefiable ground." *Géotechnique* 69 (5): 406–419. https://doi.org/10.1680/jgeot.17.P.174.

Burbank, M., T. Weaver, R. Lewis, T. Williams, B. Williams, and R. Crawford. 2013. "Geotechnical tests of sands following bioinduced calcite precipitation catalyzed by indigenous bacteria." *J. Geotech. Geoenviron. Eng.* 139 (6): 928–936. https://doi.org/10.1061/(ASCE)GT.1943-5606.0000781.

Butron, C. 2005. "Mechanical behaviour of silica Sol: Laboratory studies under controlled stress conditions during the first five months of hardening process." Master' thesis, Dept. of Civil and Environmental Engineering, Division of GeoEngineering and Geology, Chalmers Univ. of Technology.

Canterbury Development Corporation. 2014. *Christchurch economic infrastructure situation report 2014*. Christchurch, New Zealand: Canterbury Development Corporation.

CEN (European Committee for Standardization). 2004. *Geotechnical design. Part 1: General rules*. EN 1997-1, Eurocode 7. Brussels, Belgium: CEN.

Chang, W., E. M. Rathje, K. H. Stokoe, and B. R. Cox. 2004. "Direct evaluation of effectiveness of prefabricated vertical drains in liquefiable sand." *Soil Dyn. Earthquake Eng.* 24 (9–10): 723–731. https://doi.org/10.1016/j.soildyn.2004.06.007.

Chiaradonna, A., G. Tropeano, A. d'Onofrio, and F. Silvestri. 2018a. "Development of a simplified model for pore water pressure build-up induced by cyclic loading." *Bull. Earthquake Eng.* 16 (9): 3627–3652. https://doi.org/10.1007/s10518-018-0354-4.

Chiaradonna, A., G. Tropeano, A. d'Onofrio, and F. Silvestri. 2018b. "Interpreting the deformation phenomena of a levee damaged during the 2012 Emilia earthquake." *Soil Dyn. Earthquake Eng.* 124 (Sep): 389–398. https://doi.org/10.1016/j.soildyn.2018.04.039.

Consoli, N. C., D. Winter, H. B. Leon, and H. C. Scheuermann Filho. 2018. "Durability, strength, and stiffness of green stabilized sand." *J. Geotech. Geoenviron. Eng.* 144 (9): 04018057. https://doi.org/10.1061/(ASCE)GT.1943-5606.0001928.

Croce, P., A. Flora, and G. Modoni. 2014. *Jet grouting: Technology, design and control*. Boca Raton, FL: CRC Press.

Cubrinovski, M. 2013. "Liquefaction-induced damage in the 2010–2011 Christchurch (New Zealand) earthquakes." In *Proc., 7th Int. Conf. on Case Histories in Geotechnical Engineering*. Columbia, MO: Univ. of Missouri.

D'Appolonia, E. 1954. "Loose sands—Their compaction by vibroflotation." In *Proc., STP156-EB Symp. on Dynamic Testing of Soils*. West Conshohocken, PA: ASTM.

D'Apuzzo, M., A. Esposito, A. Evangelisti, R.-L. Spacagna, L. Paolella, and G. Modoni. 2019. "Strategies for the assessment of risk induced by seismic liquefaction on road networks." In *Proc., of the 29th European Safety and Reliability Conference*, edited by B. Michael and Z. Enrico. Singapore: Research Publishing Services.

Donovan, N. C., A. M. Becker, and G. Y. Lau. 1984. "Liquefaction mitigation by site improvement—A case study." In Vol. of *Proc., 8th World Conf. on Earthquake Engineering*, 693–700. Upper Saddle River, NJ: Prentice Hall.

Dyvik, R., and C. Madshus. 1985. "Lab measurements of G_{max} using bender elements." In *Proc., Advances in the Art of Testing Soils Under Cyclic Conditions*, 186–197. Reston, VA: ASCE.

El Mohtar, C. S., A. Bobet, M. C. Santagata, V. P. Drnevich, and C. T. Johnston. 2013. "Liquefaction mitigation using bentonite suspensions." *J. Geotech. Geoenviron. Eng.* 139 (8): 1369–1380. https://doi.org/10.1061/(ASCE)GT.1943-5606.0000865.

Ferreira, C., A. Viana da Fonseca, F. Diaz-Duran, and G. Cascante. 2019. "New developments in bender element testing." In *Proc., 7th Int. Conf. on Earthquake Geotechnical Engineering*. Boca Raton, FL: CRC Press, Taylor and Francis Group.

Fioravante, V., et al. 2013. "Earthquake geotechnical engineering aspects of the 2012 Emilia Romagna earthquake (Italy)." In *Proc., 7th Int. Conf. on Case Histories in Geotechnical Engineering*. Madison, WI: Omnipress.

Gallagher, P. M. 2000. "Passive site remediation for mitigation of liquefaction risk." Ph.D. thesis, Dept. of Civil and Environmental Engineering, Virginia Tech.

Gallagher, P. M., and Y. Lin. 2009. "Colloidal silica transport through liquefiable porous media." *J. Geotech. Geoenviron. Eng.* 135 (11): 1702–1712. https://doi.org/10.1061/(ASCE)GT.1943-5606.0000123.

Gallagher, P. M., and J. K. Mitchell. 2002. "Influence of colloidal silica grout on liquefaction potential and cyclic undrained behavior of loose sand." *Soil Dyn. Earthquake Eng.* 22 (9): 1017–1026. https://doi.org/10.1016/S0267-7261(02)00126-4.

Green, R. A., and G. A. Terri. 2005. "Number of equivalent cycles concept for liquefaction evaluations—Revisited." *J. Geotech. Geoenviron. Eng.* 131 (4): 477–488. https://doi.org/10.1061/(ASCE)1090-0241(2005)131:4(477).

Hamderi, M., and P. M. Gallagher. 2013. "An optimization study on the delivery distance of colloidal silica." *Sci. Res. Essays* 8 (27): 1314–1323. https://doi.org/10.5897/SRE11.2034.

Han, J. 2015. *Principles and practice of ground improvement*. New York: Wiley.

Hench, L. L. 1998. *Sol-gel silica: Properties, processing and technology transfer.* Norwich, NY: William Andrew.

Huang, Y., and L. Wang. 2016. "Laboratory investigation of liquefaction mitigation in silty sand using nanoparticles." *Eng. Geol.* 204 (Apr): 23–32. https://doi.org/10.1016/j.enggeo.2016.01.015.

Iler, R. K. 1979. *The chemistry of silica: Solubility, polymerization, colloid and surface properties, and biochemistry of silica*. New York: Wiley.

Iolli, S., G. Modoni, G. Chiaro, and E. Salvatore. 2015. "Predictive correlations for the compaction of clean sands." *Transp. Geotech.* 4 (Sep): 38–49. https://doi.org/10.1016/j.trgeo.2015.06.004.

Irfan, M., G. Cascante, and D. Basu. 2019. "Evaluation of bender transmitter response inside soil using novel laser measurements." In *Proc., 7th Int. Conf. on Earthquake Geotechnical Engineering*. Boca Raton, FL: CRC Press, Taylor and Francis Group.

Ishihara, K. 1993. "Liquefaction and flow failure during earthquakes." *Géotechnique* 43 (3): 351–451. https://doi.org/10.1680/geot.1993.43.3.351.

JGS (Japanese Geotechnical Society). 1998. *Remedial measures against soil liquefaction from investigation and design to implementation*. Rotterdam, Netherlands: A.A. Balkema.

Karol, R. H. 1968. "Chemical grouting technology." *J. Soil Mech. Found. Eng.* 94 (1): 175–204.

Kirsch, K., and A. Bell. 2012. *Ground improvement*. 3rd ed. Boca Raton, FL: CRC Press.

Kirsch, K., and F. Kirsch. 2016. *Ground improvement by deep vibratory methods*. 2nd ed. Boca Raton, FL: CRC Press.

Klug, H. P., and L. E. Alexander. 1974. *X-ray diffraction procedures: For polycrystalline and amorphous materials*. Hoboken, NJ: Wiley.

Ladd, R. S. 1978. "Preparing test specimens using undercompaction." *Geotech. Test. J.* 1 (1): 16–23. https://doi.org/10.1520/GTJ10364J.

Lee, J. S., and J. C. Santamarina. 2005. "Bender elements: Performance and signal interpretation." *J. Geotech. Geoenviron. Eng.* 131 (9): 1063–1070. https://doi.org/10.1061/(ASCE)1090-0241(2005)131:9(1063).

Liao, H. J., C. C. Huang, and B. S. Chao. 2003. "Liquefaction resistance of a colloid silica grouted sand." In *Proc., 3rd Int. Conf. on Grouting and Ground Treatment*, edited by L. F. Johnsen, D. A. Bruce, and M. J. Byle, 1305–1313. Reston, VA: ASCE. https://doi.org/10.1061/9780784406632.

Lyman, A. K. B. 1941. "Compaction of cohesionless foundation soils by explosives." *Proc. Am. Soc. Civ. Eng.* 67 (5): 769–780.

Manassero, V., and G. Di Salvo. 2012. "Two difficult tunnelling problems solved by using permeation grouting: The excavation of submerged large size tunnels for Roma and Napoli metro projects." In *Proc., 4th Int. Conf. on Grouting and Deep Mixing*, edited by L. F. Johnsen, D. A. Bruce, and M. J. Byle, 1972–1984. Reston, VA: ASCE.

Mayne, P. W., J. S. Jones Jr., and J. C. Dumas. 1984. "Ground response to dynamic compaction." *J. Geotech. Eng.* 110 (6): 757–774. https://doi.org/10.1061/(ASCE)0733-9410(1984)110:6(757).

Mele, L., J. T. Tian, S. Lirer, A. Flora, and J. Koseki. 2018. "Liquefaction resistance of unsaturated sands: Experimental evidence and theoretical interpretation." *Géotechnique* 69 (6): 541–553. https://doi.org/10.1680/jgeot.18.P.042.

Modoni, G., M. Albano, E. Salvatore, and J. Koseki. 2018. "Effects of compaction on the seismic performance of embankments built with gravel." *Soil Dyn. Earthquake Eng.* 106: 231–242.

Modoni, G., A. Flora, C. Mancuso, C. Viggiani, and F. Tatsuoka. 2000. "Evaluation of gravel stiffness by pulse wave transmission tests." *Geotech. Test. J.* 23 (4): 506–521.

Modoni, G., R. L. Spacagna, L. Paolella, E. Salvatore, A. Rasulo, and L. Martelli. 2019. "Liquefaction risk assessment: Lesson learned from a case study." In *Proc., 7th Int. Conf. on Earthquake Geotechnical Engineering*. Boca Raton, FL: CRC Press, Taylor and Francis Group.

Mori, L., M. Mooney, and M. Cha. 2018. "Characterizing the influence of stress on foam conditioned sand for EPB tunneling." *Tunnelling Underground Space Technol.* 71 (Jan): 454–465. https://doi.org/10.1016/j.tust.2017.09.018.

Moridis, G., J. Apps, P. Persoff, L. Myer, S. Muller, K. Pruess, and P. Yen. 1996. *A field test of a waste containment technology using a new generation of injectable barrier liquids*. Rep. No. LBNL-38817. Berkeley, CA: Lawrence Berkeley National Laboratory.

Mortensen, B. M., and J. T. Dejong. 2011. "Strength and stiffness of MICP treated sand subjected to various stress paths." In *Proc., Geo-Frontiers Congress 2011*. Reston, VA: ASCE.

Nguyen, T. V., D. Rayamajhi, R. W. Boulanger, S. A. Ashford, J. Lu, A. Elgamal, and L. Shao. 2012. "Effects of DSM grids on shear stress distribution in liquefiable soil." In *Proc., GeoCongress 2012, State of the Art and Practice in Geotechnical Engineering*, edited by R. D. Hryciw, A. Athanasopoulos-Zekkos, and N. Yesiller, 1948–1957. Reston, VA: ASCE.

Park, S. S., Z. An, S. R. Ye, S. B. Lee, and K. H. Chae. 2015. Vol. 17 of *Geophysical Research Abstracts*, EGU2015-10291. Munich, Germany: European Geosciences Union.

Pedrotti, M., C. Wong, G. El Mountassir, and R. J. Lunn. 2017. "An analytical model for the control of silica grout penetration in natural groundwater systems." *Tunnelling Underground Space Technol.* 70 (Nov): 105–113. https://doi.org/10.1016/j.tust.2017.06.023.

Persoff, P., J. A. Apps, and G. J. Moridis. 1999. "Effect of dilution and contaminants on strength and hydraulic conductivity of sand grouted with colloidal silica gel." *J. Geotech. Geoenviron. Eng.* 125 (6): 461–469. https://doi.org/10.1061/(ASCE)1090-0241(1999)125:6(461).

Persoff, P., G. J. Moridis, J. Apps, K. Pruess, and S. J. Muller. 1994. *Designing injectable colloidal silica barriers for waste isolation at the Hanford site. In In-situ remediation: Scientific basis for current*

and future technologies. Vienna, Austria: International Atomic Energy Agency.

Porcino, D., V. Marcianò, and R. Granata. 2011. "Undrained cyclic response of a silicate grouted sand for liquefaction mitigation purposes." *Geomech. Geoeng.* 6 (3): 155–170. https://doi.org/10.1080/17486025.2011.560287.

Salvatore, E., E. Ando, R. Proia, G. Modoni, and G. Viggiani. 2018. "Effect of strain localization on the response of granular materials subjected to monotonic and cyclic triaxial tests." *Ital. Geotech. J.* 52 (2): 30–43.

Salvatore, E., E. Andò, G. Modoni, and Viggiani, G. 2016. "Micromechanical study of cyclically loaded sands with x-ray microtomography and digital image correlation." *Procedia Eng.* 158: 92–97.

Salvatore, E., G. Modoni, E. Andò, M. Albano, and G. Viggiani. 2017. "Determination of the critical state of granular materials with triaxial tests." *Soils Found.* 57 (5): 733–744. https://doi.org/10.1016/j.sandf.2017.08.005.

Salvatore, E., R. L. Spacagna, E. Andò, and M. Ochmanski. 2019. "Geostatistical analysis of strain localization in triaxial tests on sand." *Géotech. Lett.* 9 (4): 334–339. https://doi.org/10.1680/jgele.18.00228.

Seed, H. B., I. M. Idriss, F. Makdisi, and N. Banerjee. 1975. *Representation of, irregular stress time histories by equivalent uniform stress series in liquefaction analysis*. Rep. No. EERC 75-29. Berkeley, CA: Earthquake Engineering Research Center, College of Engineering, Univ. of California.

Shirley, D. J., and L. D. Hampton. 1978. "Shear-wave measurements in laboratory sediments." *J. Acoust. Soc. Am.* 63 (2): 607–613. https://doi.org/10.1121/1.381760.

Spagnoli, G. 2018. "A review of soil improvement with non-conventional grouts." *Int. J. Geotech. Eng.* 1–15. https://doi.org/10.1080/19386362.2018.1484603.

Sydansk, R. D. 1990. "A newly developed chromium(III) technology." *SPE Reservoir Eng.* 5 (3): 346–352. https://doi.org/10.2118/19308-PA.

Tonkin + Taylor. "Liquefaction damage to Christchurch/Canterbury from series of earthquakes during 2010–2011." Posted May 9, 2016. YouTube video. https://www.youtube.com/watch?v=rH-UUx5W1rw.

Towhata, I. 2008. *Geotechnical earthquake engineering*. Berlin: Springer Science & Business Media.

Traldi, D., and P. Levanto. 2016. "Metodi innovativi per il consolidamento e l'impermeabilizzazione in sotterraneo." *Ingegno* 47.

Wang, Z., J. Ma, H. Gao, A. W. Stuedlein, J. He, and B. Wang. 2019. "Unified thixotropic fluid model for soil liquefaction." *Géotechnique* 1–14. https://doi.org/10.1680/jgeot.17.P.300.

Xiao, P., H. Liu, A. W. Stuedlein, and T. M. Evans. 2019. "Effect of relative density and biocementation on cyclic response of calcareous sand." *Can. Geotech. J.* 56 (12): 1849–1862. https://doi.org/10.1139/cgj-2018-0573.

Xiao, P., H. Liu, Y. Xiao, A. W. Stuedlein, and T. M. Evans. 2018a. "Liquefaction resistance of bio-cemented calcareous sand." *Soil Dyn. Earthquake Eng.* 107 (Apr): 9–19. https://doi.org/10.1016/j.soildyn.2018.01.008.

Xiao, Y., A. M. Stuedlein, Q. Chen, H. Liu, and P. Liu. 2018b. "Stress-strain-strength response and ductility of gravels improved by polyurethane foam adhesive." *J. Geotech. Geoenviron. Eng.* 144 (2): 04017108. https://doi.org/10.1061/(ASCE)GT.1943-5606.0001812.

Yamauchi, T., H. Tezuka, and Y. Tsukamoto. 2017. "Development of rational soil liquefaction countermeasure consisting of lattice-shaped soil improvement by jet grouting for existing housing estates." In *Proc., Geotechnical Hazards from Large Earthquakes and Heavy Rainfalls*, edited by H. Hazarika, M. Kazama, and W. F. Lee, 49–59. Tokyo: Springer.

Yasuda, S., K. Harada, K. Ishikawa, and Y. Kanemaru. 2012. "Characteristics of liquefaction in Tokyo Bay area by the 2011 Great East Japan earthquake." *Soils Found.* 52 (5): 793–810. https://doi.org/10.1016/j.sandf.2012.11.004.

Yegian, M. K., E. Eseller-Bayat, A. Alshawabkeh, and S. Ali. 2007. "Induced-partial saturation for liquefaction mitigation: Experimental investigation." *J. Geotech. Geoenviron. Eng.* 133 (4): 372–380. https://doi.org/10.1061/(ASCE)1090-0241(2007)133:4(372).

Yonekura, R. 1996. "The developing process and the new concepts of chemical grout in Japan." In *Proc., IS-Tokyo'96, the 2nd Int. Conf. on Ground Improvement Geosystems*, edited by R. Yonekura, M. Shibazaki, and M. Terashi, 889–901. Rotterdam, Netherlands: A.A. Balkema.

Yonekura, R., and M. Miwa. 1993. "Fundamental properties of sodium silicate based grout." In *Proc., 11th Southeast Asian Geotechnical Conf.*, edited by S. L. Lee, K. Y. Tong, and Y. K. Chow, 439–444. Boca Raton, FL: Taylor and Francis Group.

Ziotopoulou, K., and R. W. Boulanger. 2013. "Calibration and implementation of a sand plasticity plane-strain model for earthquake engineering applications." *Soil Dyn. Earthquake Eng.* 53 (Oct): 268–280. https://doi.org/10.1016/j.soildyn.2013.07.009.